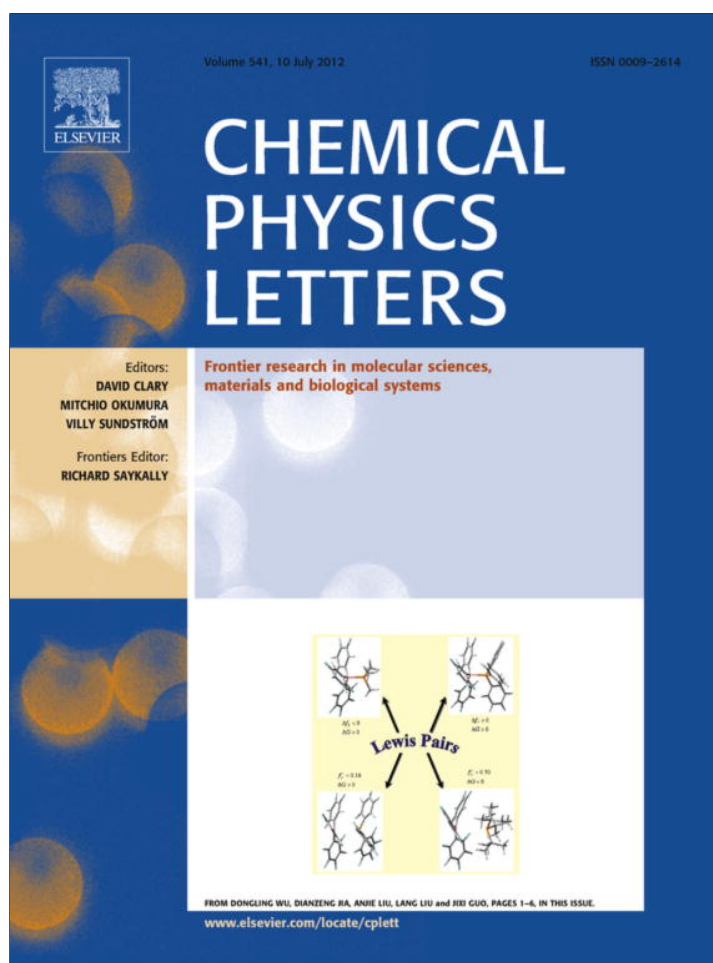


Provided for non-commercial research and education use.
Not for reproduction, distribution or commercial use.



This article appeared in a journal published by Elsevier. The attached copy is furnished to the author for internal non-commercial research and education use, including for instruction at the authors institution and sharing with colleagues.

Other uses, including reproduction and distribution, or selling or licensing copies, or posting to personal, institutional or third party websites are prohibited.

In most cases authors are permitted to post their version of the article (e.g. in Word or Tex form) to their personal website or institutional repository. Authors requiring further information regarding Elsevier's archiving and manuscript policies are encouraged to visit:

<http://www.elsevier.com/copyright>

Contents lists available at [SciVerse ScienceDirect](#)

Chemical Physics Letters

journal homepage: www.elsevier.com/locate/cplett

Improved fast photoresponse from Al doped ZnO nanowires network decorated with Au nanoparticles

Soumen Dhara^a, P.K. Giri^{a,b,*}^a Department of Physics, Indian Institute of Technology Guwahati, Guwahati 781039, India^b Centre for Nanotechnology, Indian Institute of Technology Guwahati, Guwahati 781039, India

ARTICLE INFO

Article history:

Received 28 February 2012

In final form 13 May 2012

Available online 30 May 2012

ABSTRACT

Herein we report an effective novel approach to improve the photoresponse and reset times as well as the photosensitivity of the ZnO NWs heterostructure. We show that as compared to the pristine ZnO NWs, much faster photoresponse (100 ms) and enhanced (sixfolds) photosensitivity could be achieved by Al doping followed by Au NPs decoration of the ZnO NWs networks. The improvement in the photosensitivity and photoresponse time is explained on the basis of plasmon assisted electrons transfer from Au NPs to ZnO NWs and interfacial interaction with the photogenerated electrons.

© 2012 Elsevier B.V. All rights reserved.

1. Introduction

In modern days, the UV photodetectors have a wide range of applications in various fields, ranging from environmental UV radiation monitoring, space research, high temperature flame detection to optical communications [1]. High photosensitivity and selectivity, faster response and reset times, and reproducible characteristics are the basic requirements for an efficient photodetector [2,3]. ZnO nanowires (NWs) are considered to be one of the best materials for the application in UV photodetectors due its very high absorption in the UV region and large surface-to-volume ratio. The small physical size of the NWs and the ability to integrate into the mainstream Si based electronics makes it a better candidate for future large-scale optoelectronic integration. A number of attempts have been made to study the photodetection behavior of the bare ZnO NWs (single NW or NWs array) by several research groups [2,4–8]. Detailed investigations have also been carried out to understand the mechanism of the observed photodetection of the ZnO NWs. Kind et al. [4] first pointed out the involvement of oxygen adsorption and photodesorption processes in the photodetection behavior of ZnO NWs and later this concept was further elaborated by other researchers [7,9–11]. From their studies, Kind et al. concluded that the single ZnO NW based devices have comparatively faster response. However, due to low photocurrent (PC) it does not find applications in the real world. Fabrication of photodetectors by using large numbers of ZnO NWs could be an alternative; however, integration and collective electrical contacts to a large number of NWs is a critical issue [12,13]. The best way to

achieve integration of large number of NWs is a direct growth technique. In this method, ZnO NWs arrays are grown on the suitable substrate and then it is used as photodetector by making electrical contacts with low contact resistance. This type of photodetector gives very high photocurrent. However, the photoresponse and reset times (defined as the time requires to reach $1-1/e$ (63%) and recovery to $1/e$ (37%) of the maximum photocurrent, respectively) are very slow, ranging from few seconds to several hundred seconds [5,14]. Earlier, most of the studies were aimed to improve the photosensitivity and investigated the origin of enhanced PC. As the density of the surface defect states influence the photocarrier generation and lifetime, researchers have fabricated varieties of ZnO NWs based heterostructures by surface modification and achieved significant improvement in photosensitivity [15–18]. For example, when the NWs' surfaces are capped with an inorganic semiconducting material (zinc sulfide) [15] or with an organic polymer (polyvinyl alcohol) [16], the PC gain has been enhanced by 3–4 times due to reduced effect of the carrier relaxation during steady UV illumination. In our recent studies, we achieved very high photosensitivities from arrays of ZnO NWs heterostructures, one made with Au nanoparticles (NPs) decoration [19] and other with anthracene capping [20]. However, very little works have been made on the improvement of the photoresponse and reset times. To improve the photoresponse and reset times, combination of Schottky contact and surface functionalization [21], metal (Ag, Al) doping [22,23] have been recently employed.

Here we report an effective approach to improve the photoresponse and reset times as well as the photosensitivity of the ZnO NWs heterostructure and investigated the combined effects of Al doping and Au nanoparticles (NPs) decoration. Much faster photoresponse and reset times (100 and 110 ms), and enhanced

* Corresponding author at: Department of Physics, Indian Institute of Technology Guwahati, Guwahati 781039, India.

E-mail address: giri@iitg.ernet.in (P.K. Giri).

photosensitivity were obtained by the combined effect of Al doping and Au NPs decoration on the surface of the ZnO NWs network. The absorption and photoluminescence (PL) spectra are also carefully studied to understand the improvement in the photoresponse and reset times.

2. Experimental details

The Al doped ZnO NWs (Al:ZnO NWs) network of two different concentration of Al (3% and 6%) were grown on the oxidized Si wafer substrate by vapor–liquid–solid process in an in-house developed thermal vapor deposition system. Al doped ZnO powder as a source and Au coated (~ 2 nm thick) oxidized Si as a substrate were used during the growth of the NWs. 3% and 6% Al doped ZnO powder was prepared by using mechanical ball milling process. Commercial high purity ZnO powder (purity 99.999%, Sigma Aldrich) and Al powder (99.7%, Loba Chemie) were used as starting materials. First 3% Al powder was mixed properly with ZnO powder and then ball-milling was performed at 300 rpm for a duration of 5 h in a zirconia vial (Retsch, PM100) under atmospheric condition using small zirconium balls at a weight ratio of 10:1 for powder mixture. The 6% Al doped powder was prepared by a similar process. The uniform doping of Al in the as-prepared ZnO powder was confirmed by X-ray diffraction (XRD, Seifert 3003 T/T) using a Mo X-ray gun ($\lambda = 0.7093$ Å) measurement and energy-dispersive X-ray spectroscopy (EDX) scanning. The XRD patterns do not shows any segregation of Al in the doped powder. For the growth of Al:ZnO NWs, as-prepared doped powder and graphite powders (purity 99.99%, Fluka) mixture was used as ZnO vapor source material and placed inside a horizontal muffle furnace. The ZnO vapor was formed at 950 °C and was deposited on the Au coated oxidized Si substrate at 700 °C for 30 min. The chamber pressure was maintained at 1.3 mbar during the growth. Field emission scanning electron microscopy (FESEM, Sigma, Zeiss) was used to confirm the formation of ZnO NWs. The crystal structure of the NWs was characterized by XRD and transmission electron microscopy (TEM, JEM2100, JEOL) with selected area electron diffraction (SAED). Raman scattering measurement was carried out with a 488 nm Ar⁺ laser excitation using a micro-Raman spectrometer (LabRAM HR-800, Jobin Yvon) equipped with a liquid nitrogen-cooled charge-coupled device detector. To further improve the photoresponse and photosensitivity, 3% doped Al:ZnO NWs sample was broken into two pieces and one piece is used for the decoration of ultra small Au NPs on the surface of the Al:ZnO NWs by sputter deposition process. The Au sputtering was done at 1 kV DC voltage for 180 s, which results in an estimated 25 Å thick Au layer. From our previous study [19], it is found that this thickness is optimum for the maximum improvement in the PC in the ZnO NWs. The specular reflectance (angle of incidence 45°) of the Al:ZnO NWs were measured using a UV–Vis spectrometer (Varian Carry 50, Varian). The PL spectra of all the samples were recorded at room temperature with a 325 nm He–Cd laser excitation using a high-resolution commercial PL spectrometer (FS 920P, Edinburg Instruments).

For the PC measurements, two circular Al contacts of 100 nm thickness were made on the NWs by thermal evaporation process using shadow mask. The diameter of the circular electrodes is ~ 350 μm with a fixed separation of 2.5 mm between the electrodes. The photoresponse was measured using a picoammeter (Keithley, Model 6487) at a bias of 3 V under the illumination of monochromated UV light (wavelength 365 nm) from a 150 W xenon lamp at a light intensity of ~ 0.5 mW/cm² in ON and OFF conditions. The UV light is tightly focused onto the sample making sure that the region between the two electrodes is only illuminated. All the measurements were carried out at room temperature and atmospheric pressure.

3. Results and discussion

Figure 1a shows the FESEM image of the 6% Al:ZnO NWs grown on the oxidized Si(100) substrate. The NWs grew horizontally along the substrate plane and form a network like structure where each one is connected with the other nearest neighbor NWs. These NWs are very thin with diameter ranging from 10 to 16 nm and length in the range of 0.6–1.0 μm . The EDX spectrum (Figure 1b) confirms the presence of Al in the Al:ZnO NWs sample. The 3% Al:ZnO NWs shows similar morphology with average diameter 12 nm. Figure 1c shows the typical TEM image of the 6% Al:ZnO NWs. The measured diameter of the NWs is in the range of 11–16 nm, which is in close agreement with the diameter obtained from the FESEM image. The inset shows the SAED pattern of the corresponding single NW, which clearly shows the intense diffraction spot of (002) planes. Figure 1d shows the high-resolution TEM lattice image taken from one end of 6% doped single NW (shown by dotted rectangle). The long white arrow shows the growth direction of the NW. The measured lattice spacing is 2.58 Å, which corresponds to the (002) plane. Therefore, the SAED pattern and lattice image confirm the one-dimensional single-crystalline structure of the Al:ZnO NWs. Compared to the d_{002} spacing (2.61 Å) of the bulk ZnO, the obtained d_{002} spacing in the present case is smaller. Therefore, the Al:ZnO NWs are found to be strained and the nature of strain is compressive.

Further, structural characterization of the Al:ZnO NWs was done by XRD measurements. Figure 2 shows the XRD patterns of the 3% and 6% doped Al:ZnO NWs, which show characteristic peaks of crystalline hexagonal phase of ZnO. No other peaks related to the Al or aluminium oxide are detected. The observed strong peak corresponds to the ZnO(002) planes, which further confirmed the highly crystalline nature of the sample. Exact position of the (002) peak is calculated from the Lorentzian fitting to the experimental data. It is found that the peak position is slightly shifted towards higher 2θ . This up shift indicates lower lattice spacing and it implies that the fabricated Al:ZnO NWs are strained compressively, which is fully consistent with the HRTEM results. It is also noticed that the compressive strain increases with increase in Al concentration, as expected. In case of Al doping in ZnO, it is known that the Al atoms occupy the Zn lattice site due to almost identical covalent radius of Al atom (121 pm) and the Zn atom (122 pm).

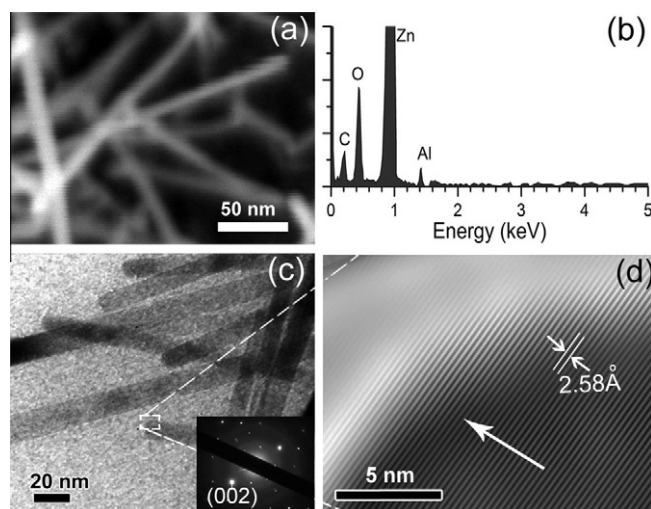


Figure 1. (a) FESEM image of the Al doped (6%) as-grown ZnO NWs network with an average diameter 12 nm and (b) the corresponding EDX spectra of the above NWs, confirming the presence of Al in the NWs. (c) TEM image of the above Al:ZnO NWs and the inset shows the corresponding SAED pattern of one of the single NW. (d) High resolution TEM lattice image of the NW taken from one end of the NW.

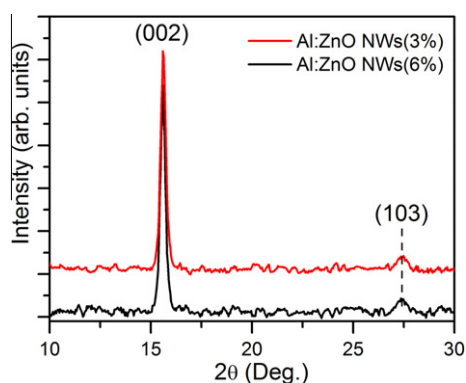


Figure 2. XRD patterns of the 3% and 6% Al doped ZnO NWs, showing the c-axis orientation of the ZnO NWs.

Therefore, the incorporation of Al atoms into ZnO leads to slight decrease of lattice constants in ZnO, resulting in the compressive strain in the Al:ZnO NWs. It is known that, strain has a strong effect on the optical properties, as it directly influences the band gap of the material. Compressive strain usually leads to increase in the band gap and the tensile strain leads to decrease in the band gap [24,25]. Therefore, a change in optical properties with band gap widening is expected from the Al:ZnO NWs.

The structural quality of the Al:ZnO NWs was further evaluated by micro-Raman analysis. Figure 3 shows the Raman spectra of the 3% and 6% Al:ZnO NWs. The Raman spectra show characteristic Raman modes of hexagonal ZnO with good crystallinity. The Raman peaks at ~ 332 , ~ 381 and ~ 438 cm^{-1} correspond to $2E_2$, A_1^{TO} and E_2^{high} modes of hexagonal ZnO, respectively [26]. The strong E_2^{high} mode indicates the highly crystalline structure of the as-grown Al:ZnO NWs. It is also observed that with increase in Al concentration, the intensity of the E_2^{high} mode decreases. The observed reduction in intensity indicates the deterioration of crystalline quality of the doped NWs. Besides the common hexagonal ZnO modes, two additional modes are observed from both the samples, one at 620 nm and other at 680 nm. The intensity of the above two peaks are found to increase with the increase in Al concentration. In general, it has been reported that doping causes structural disorder in the host lattice. Therefore, above two peaks can be attributed to the structural disorder related vibrations, as both these modes are not associated with the Raman modes of Al. Here, as the doping concentration is increased, the substitution of dopant into the Zn lattice can cause strain and the oxygen in the ZnO host lattice can be shared by both Zn and Al. This will lead to neighboring disorder and local geometric disorientation, as result it increases

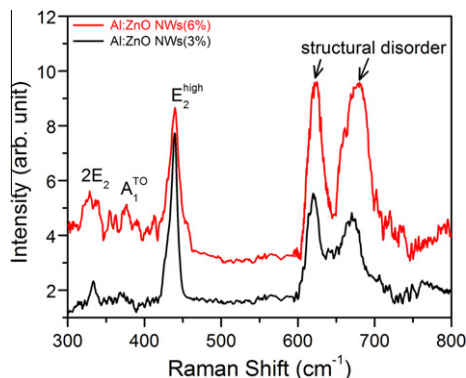


Figure 3. Micro-Raman spectra of the 3% and 6% Al doped ZnO NWs. Characteristic modes are marked with standard notations.

the intensity of the disorder related peak. The strain-free ZnO bulk crystal shows E_2^{high} mode at 438 cm^{-1} . In the figure, frequency position of E_2^{high} mode for the 3% and 6% Al:ZnO NWs are at 438.1 and 438.7 cm^{-1} , respectively. It has been reported that the E_2^{high} mode is very sensitive to strain/stress state of ZnO crystal [27,28]. Therefore, upshift in the E_2^{high} mode is the result of increment in compressive biaxial strain. This is consistent with the XRD and TEM analysis. Similar compressive strain has been reported in the Al doped ZnO thin films [29].

Figure 4a shows the dark current–voltage (I – V) characteristics of the 3% and 6% doped Al:ZnO NWs. As each of the NWs is connected with the nearest neighbor, current carriers can easily flow from one NW to the other by tunneling process through the junction between the NWs. I – V characteristics show nearly linear behavior with comparatively higher dark current than the undoped NWs. In our previous studies, we found that the dark current of the undoped ZnO NWs varies in the range 2–10 nA [11,19]. However, in the present case they obtained dark current is more than one order of magnitude higher and it increases with the increase in doping concentration. At a bias of 3 V, the dark current increases from 110 to 180 nA when the Al concentration increases from 3% to 6%. The higher dark current is primarily due to the increase in free carrier concentration due to doping of Al in the ZnO lattice. Here trivalent Al^{3+} ions contribute to the enhanced current conduction process by increasing the free electron density in the doped NWs. On the other hand, the Al:ZnO/Au NWs shows a reduction in the dark current to 70 nA due to the upward band bending at the interface between Au and ZnO. The upward energy band bending occurs at the interface due to the differences in work function of ZnO (4.65 eV) and Au (5.47 eV), and the band bending affects the dark current. In our earlier study, we have discussed the effects of band bending on the dark current for different interfaces [19].

The photoresponse of the Al:ZnO NWs measured under the excitation of 365 nm UV light is shown in Figure 4b–d. The obtained response and reset times are below one second, which is comparatively faster than the response time of the undoped ZnO NWs (several seconds). For the 3% doped Al:ZnO NWs (see Figure 4b), the maximum photocurrent is about 5.3 μA , leading to the photosensitivity of 50. With further doping (6%), the maximum obtained PC does not change significantly. This is because the maximum PC depends on the numbers of photocarriers generated

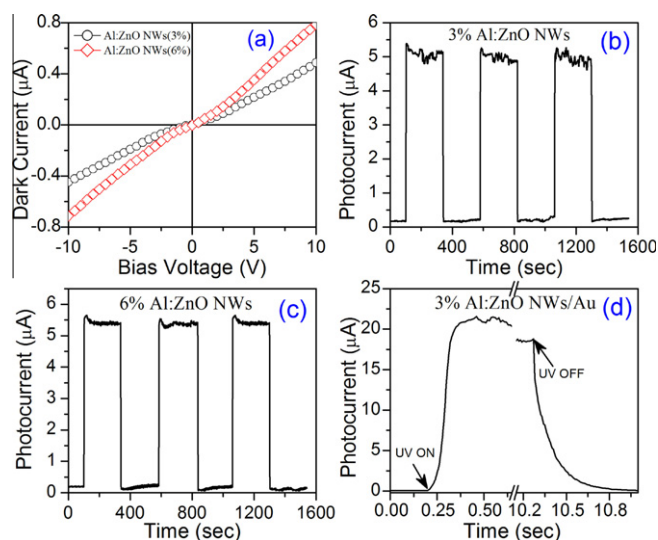


Figure 4. (a) Dark current–voltage characteristics of the 3% and 6% Al doped ZnO NWs. (b and c) Reproducible photoresponse behaviors (at 365 nm) of the above two samples. (d) Photoresponse of the 3% Al doped NWs after the surface decoration with Au NPs.

between the conduction band and valence band. This is further indicates that the doping concentration does not have any strong effect on the density of photocarriers generated. Although these NWs show a high increment in the photocurrent under the UV excitation, the photosensitivity values are actually very low due to the high dark current. Our results are similar to the previous reports on Al:ZnO NWs [23,30,31]. This relatively low photosensitivity from the Al:ZnO NWs hinders the fabrication and development of highly efficient UV photodetectors. However, in the present case, the photoresponse and reset times are very fast compared to the as-grown undoped ZnO NWs or NWs heterostructures. The photoresponse and reset times of the Al:ZnO NWs show a dependence on Al concentration. At low doping level of Al, the photoresponse and reset times are significantly reduced. The 3% doped Al:ZnO NWs shows photoresponse and reset times of 0.9 and 1.1 s, respectively (Figure 4b). Higher doping shows further reduction, though small, in the photoresponse and reset times, as shown in Figure 4c. Therefore, Al doping accelerates the photocurrent saturation rate, which indicates that the oxygen re-adsorption rate reached equilibrium instantly. Earlier, similar improvements in the photoresponse and reset times are reported for Ag doped ZnO NWs [22]. In order to improve the photosensitivity of the Al:ZnO NWs, we decorated the surface of the 3% doped Al:ZnO NWs by small Au NPs. The Al:ZnO/Au NWs shows a significant improvement in the UV photosensitivity with an enhancement factor of six (Figure 4d). The obtained photosensitivity is 300. At the same time, the photoresponse and reset times are also significantly reduced, which results in an ultra fast photodetection. The obtained photoresponse and reset times of 100 and 110 ms, respectively. Therefore, after the Au NPs decoration, the photoresponse and reset times are about one order of magnitude faster, which is a very significant improvement. Thus, the Au NPs decorated Al:ZnO NWs are found to a strong candidate for the fabrication of much faster UV photodetectors.

To understand further the origin of enhanced photoconduction behavior of the Al:ZnO NWs, we studied the optical absorption and emission properties by measuring the room temperature specular reflectance and PL spectra. The absorption spectra are calculated from their corresponding reflectance spectra according to the method proposed by Rusil et al. [32]. The UV–Vis absorption spectra of the Al:ZnO NWs is shown in Figure 5a. Absorption spectra show a sharp UV absorption and constant blue shift in absorption

edge as a function of Al doping concentration. Compared to the absorption edge of undoped ZnO NWs (367 nm) [11], 3% doped NWs show absorption edge at 364 nm and with higher doping, it is shifted towards lower wavelength. The observed blue shift indicates a band gap widening in the Al:ZnO NWs due to the Al incorporation. This is consistency with the XRD results, which indicates a possible band gap widening due to the presence of compressive strain in the Al:ZnO lattice. It is also known that, there is a possibility of band gap widening in doped semiconductors due to Burstein Moss (BM) effect. Therefore, the observed band gap widening is attributed to the combined effects of compressive strain and BM effect. The Al:ZnO NWs also show absorption in the blue–green region, which is attributed to the surface defects related absorption.

The room temperature PL spectra of the Al:ZnO and Al:ZnO/Au NWs are shown in Figure 5b–d. The 3% Al doped ZnO NWs exhibit near band edge (NBE) UV emission at ~378 nm and a broad green emission band. Gaussian multipeak fitting to the green band shows the existence of two emission bands, one at 494 nm (1st green emission) and another at 545 nm (2nd green emission). The observed NBE emission is due to bound excitonic recombination, the 1st green emission is due to the presence of oxygen vacancy states on the surface of ZnO NWs and 2nd green emission band is due to the presence of deep interstitial oxygen states inside the NWs [33]. It is found that the intensities of the UV PL as well as the green PL gradually increase with increase in Al doping concentration (Figure 5c). The PL spectra are consistent with the absorption spectra, which show enhancement in the peak intensities in the UV as well as visible region. After the Au NPs decoration on the 3% doped Al:ZnO NWs, the UV PL intensity is dramatically enhanced and green emission peak is significantly reduced, as shown in Figure 5d. Here a fourfold enhancement in the UV PL intensity is obtained from the Al:ZnO/Au NWs, while the 1st green emission intensity reduced to half and the 2nd green emission intensity is one third of its initial value. The observed UV PL enhancement is attributed to the combined effects of spontaneous recombination in ZnO and surface plasmon assisted enhanced recombination, which is explained earlier in a previous report [19]. From the absorption study of the Au NPs, it is known that the electrons in the Fermi level of Au NPs are excited by absorbing incident light in the UV–violet region due to interband transition and in the green region due to the surface plasmon resonance [34]. Subsequently, the excited energetic electrons stay in higher energy states, and these are so active that they can escape from the surface of the NPs and transfer to the conduction band of ZnO. In the present case, when the Al:ZnO/Au NWs were illuminated with UV light, the excited energetic electrons in the Au NPs can escape from the surface of the NPs and transfer to the conduction band of ZnO through the interface. The surface plasmon resonance (SPR) in Au NPs generates energetic electrons with energy larger than the energy of the conduction band of ZnO. In this case, SPR occurs through the reabsorption of the emitted green light from ZnO, which possibly reduces the green emission intensity. Subsequently these electrons can easily be injected to the conduction band of ZnO through the Au/ZnO interface and increase the electron accumulation. This process leads to the enhanced recombination probability, which results in the improvement in the UV PL intensity. This explains the enhancement in the UV PL and decrement in the green emission intensities in Al:ZnO/Au NWs. Earlier, Lin et al. [35] explained the electrons transfer process from Au to the conduction band of ZnO to account for the enhancement of UV PL intensity from the Au NPs decorated ZnO nanorods.

The obtained faster photoresponse and improved photosensitivity for the Al:ZnO/Au NWs can be explained as follows. It is known that the photoresponse of ZnO NWs depends on electron-hole generation, surface adsorption and photodesorption processes. It is also known that fast or slow response strongly depends

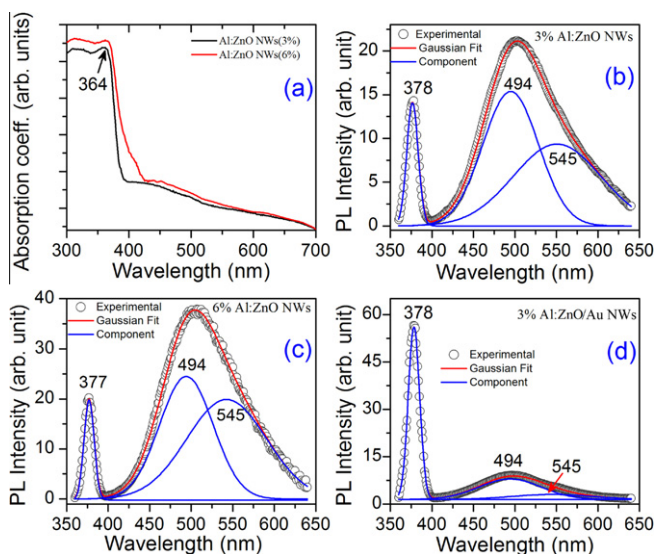


Figure 5. (a) UV–Vis absorption spectra of the 3% and 6% Al doped ZnO NWs. Room temperature PL spectra of the (b) 3% and (c) 6% Al doped ZnO NWs. (d) PL spectra of the 3% Al doped NWs after the decoration with Au NPs.

on the time taken to reach the equilibrium rate of oxygen desorption and readsorption process. In the present case, Al doping of the ZnO NWs possibly change the equilibrium defect concentration, besides changing the electron concentrations. Due to this, surface defects in the Al:ZnO NWs gradually increases with the increase in Al concentration. This is supported by the optical absorption and PL results. The optical absorption and PL data show systematic increase in the surface defects related absorption and emission in the green region. For this reason, the rates of oxygen desorption and readsorption processes are significantly improved and instantly reach the equilibrium rate. This process results in faster photoresponse in the Al:ZnO NWs. Whereas in case of Al:ZnO/Au NWs, the decoration of Au NPs induces rough surface morphology and interface states at the ZnO/Au interface. As reported previously, a larger number of oxygen molecules are adsorbed on the surfaces of rough ZnO NWs than smooth ZnO NWs [36,37]; thus, more photogenerated holes are trapped by adsorbed oxygen on the surfaces of rough ZnO NWs, suppressing the recombination of excitons under UV illumination. Therefore, the PC reached the saturation value at a much faster time, and a further improvement in the response time is obtained. Similarly, after turning off the UV, the high density of oxygen molecules adsorb on the roughened surface of ZnO NWs more quickly, presumably due to increased binding energies for oxygen adsorption on the roughened surface. As a result, much faster reset time is achieved for the Al:ZnO/Au NWs device.

The enhancement in photosensitivity in the Al:ZnO/Au NWs is due to the interband transition and surface plasmon assisted interfacial electrons transfer to the conduction band of ZnO, as explained before to explain the PL. In the present case, under UV light and external bias, the injected electrons from the Au NPs along with photogenerated electrons due to band edge absorption of ZnO contributed to the current conduction process, resulting in the enhanced photocurrent. Therefore, we believe that the enhanced photocurrent in the present case is due to the increase in electron density in the conduction band of ZnO by band edge absorption of ZnO and surface plasmon assisted interfacial electron transport from Au NPs.

4. Conclusion

Here we investigated the combined effect of Al doping and Au NPs decoration on the faster photoresponse and improved photosensitivity of the ZnO NWs. We have demonstrated that this is an effective approach to strongly improve the photoresponse and the photosensitivity of the ZnO NWs based photodetector. Without Au decoration, the doped ZnO NWs show photoresponse and reset times of 0.9 and 1.1 s, respectively, which is much faster than the case of undoped ZnO NWs. With subsequent decoration of the ultra small Au NPs on the surface of the NWs, the photoresponse and reset times are dramatically reduced to 100 and 110 ms, respectively.

The fast response is explained on the basis of change in defect equilibrium by Al doping and formation of interface traps due to Au NPs decoration. And the improvement in the photosensitivity is explained by plasmon assisted interfacial electrons transfer from Au NPs to ZnO NWs. The optical absorption and PL studies support our proposition on the mechanism of improved photoresponse. The faster photoresponse and improved photosensitivity from the Al:ZnO/Au NWs makes it a superior candidate for the fabrication of photodetectors with real time sensing.

References

- [1] E. Monroy, F. Omnes, F. Calle, *Semicond. Sci. Technol.* 18 (2003) R33.
- [2] L. Luo, Y.F. Zhang, S.S. Mao, L.W. Lin, *Sens. Actuators A, Phys.* 127 (2006) 201.
- [3] L. Vj et al., *IEEE J. Sel. Top. Quantum Electron.* 17 (2011) 1002.
- [4] H. Kind, H.Q. Yan, B. Messer, M. Law, P.D. Yang, *Adv. Mater.* 14 (2002) 158.
- [5] S.E. Ahn, J.S. Lee, H. Kim, S. Kim, B.K. Kang, K.H. Kim, G.T. Kim, *Appl. Phys. Lett.* 84 (2004) 5022.
- [6] J.Y. Park, Y.S. Yun, Y.S. Hong, H. Oh, J.-J. Kim, S.S. Kima, *Appl. Phys. Lett.* 87 (2005) 123108.
- [7] C. Soci et al., *Nano Lett.* 7 (2007) 1003.
- [8] A. Manekathodi, M.Y. Lu, C.W. Wang, L.J. Chen, *Adv. Mater.* 22 (2010) 4059.
- [9] Q.H. Li, T. Gao, Y.G. Wang, T.H. Wang, *Appl. Phys. Lett.* 86 (2005) 123117.
- [10] Y. Li, F.D. Valle, M. Simonnet, I. Yamada, J.J. Delaunaya, *Appl. Phys. Lett.* 94 (2009) 023110.
- [11] S. Dhara, P.K. Giri, *Nanoscale Res. Lett.* 6 (2011) 504.
- [12] J.S. Lee, M.S. Islam, S. Kim, *Sens. Actuators B, Chem.* 126 (2007) 73.
- [13] C.C. Huang, B.D. Pelatt, J.F. Conley, *Nanotechnology* 21 (2010) 195307.
- [14] Z.Y. Fan, D. Dutta, C.J. Chien, H.Y. Chen, E.C. Brown, P.C. Chang, J.G. Lu, *Appl. Phys. Lett.* 89 (2006) 213110.
- [15] A. Bera, D. Basak, *ACS Appl. Mater. Interfaces* 2 (2009) 408.
- [16] A. Bera, D. Basak, *ACS Appl. Mater. Interface* 1 (2009) 2066.
- [17] J. Chang, C.K. Najeeb, J.-H. Lee, M. Lee, J.-H. Kim, *J. Phys. D: Appl. Phys.* 44 (2011) 095101.
- [18] L. Guo, H. Zhang, D. Zhao, B. Yao, B. Li, Z. Zhang, D. Shen, *Mat. Lett.* 65 (2011) 1495.
- [19] S. Dhara, P.K. Giri, *J. Appl. Phys.* 110 (2011) 124317.
- [20] S. Dhara, P.K. Giri, *J. Appl. Phys.* 111 (2012) 044320.
- [21] J. Zhou et al., *Appl. Phys. Lett.* 94 (2009) 191103.
- [22] D. Lin, H. Wu, W. Zhang, H. Li, W. Pan, *Appl. Phys. Lett.* 94 (2009) 172103.
- [23] Y. Feng, W. Hou, X. Zhang, P. Lv, Y. Li, W. Feng, *J. Phys. Chem. C* 115 (2011) 3956.
- [24] C.P. Dietrich, M. Lange, F.J. Klüpfel, H.v. Wenckstern, R. Schmidt-Grund, M. Grundmann, *Appl. Phys. Lett.* 98 (2011) 031105.
- [25] S. Dhara, P.K. Giri, *Nanoscale Res. Lett.* 6 (2011) 320.
- [26] Ü. Özgür et al., *J. Appl. Phys.* 98 (2005) 041301.
- [27] T. Gruber, G.M. Prinz, C. Kirchner, R. Kling, F. Reuss, W. Limmer, A. Waag, *J. Appl. Phys.* 96 (2004) 289.
- [28] H.-W. Suh, G.-Y. Kim, Y.-S. Jung, W.-K. Choi, D. Byun, *J. Appl. Phys.* 97 (2005) 044305.
- [29] Y.-C. Cheng, *Appl. Surf. Sci.* 258 (2011) 604.
- [30] D. Lin, H. Wu, W. Pan, *Adv. Mater.* 19 (2007) 3968.
- [31] K.-P. Kim, D. Chang, S.K. Lim, S.-K. Lee, H.-K. Lyu, D.-K. Hwang, *J. Appl. Phys.* 50 (2011) 06GF07.
- [32] G.A.J. Rusli, J. Amaratunga, *Appl. Optics* 34 (1995) 7914.
- [33] B. Lin, Z. Fu, Y. Jia, *Appl. Phys. Lett.* 79 (2001) 943.
- [34] M.A. Garcia, *J. Phys. D: Appl. Phys.* 44 (2011) 283001.
- [35] H.Y. Lin, C.L. Cheng, Y.Y. Chou, L.L. Huang, Y.F. Chen, K.T. Tsen, *Opt. Express* 16 (2006) 2372.
- [36] W.K. Hong et al., *Nano Lett.* 8 (2008) 950.
- [37] W. Park et al., *Nanotechnology* 20 (2009) 475702.